Iğdır Üniversitesi Fen Bilimleri Enstitüsü Dergisi, 14(3), 1094-1110, 2024
Journal of the Institute of Science and Technology, 14(3), 1094-1110, 2024

ISSN: 2146-0574, eISSN: 2536-4618

Electrical Electronic Engineering **DOI: 10.21597/jist.1399068**

Research Article

Received: 01.12.2023 **Accepted: 18.07.2024**

To Cite: Arslan Madak, S. S., Teber, A. & Topkaya, R. (2024). Ultra-thin Polarization Converter Using Single Layer Metasurface for X-, Ku-, and K-Band Applications. *Journal of the Institute of Science and Technology*, 14(3), 1094-1110.

Ultra-thin Polarization Converter Using Single Layer Metasurface for X-, Ku-, and K-Band Applications

Seher Şeyma ARSLAN MADAK[1], Ahmet TEBER[2*], Ramazan TOPKAYA[1]

Highlights:

- Ultra-thin, broadband, single layer linear to circular and linear to linear polarization converter is designed.
- Polarization conversion ratio is achieved more than 90% from 12.57-19.30GHz.
- The suggested polarization converter can be relatively applied with beam scanning antennas.

ABSTRACT:

In this article, an ultrathin (λ_0/14.9), single layer, reflective type polarization converter for either linear-to-circular (LP-to-CP) or linear-to-linear (LP-to-LP) polarization conversion is reported. It has been demonstrated to achieve the LP-to-CP conversion at two separate frequency bands, including 11.52-11.84GHz and 19.83-20.01GHz. The circular polarization type is specified as a right-hand circular polarization (RHCP) for the first band and a left-hand circular polarization (LHCP) for the second band. In both of frequency bands, the metasurface structure reveals highly efficient features. Besides that, the metasurface structure exhibits highly efficient features within 3-dB bandwidths of 10.29-12.58GHz and 19.32-20.50GHz. Crucial parameters of polarization conversion such as ellipticity, axial ratio, and |Eco|/|Ecross| are confirmed to be in good agreement with another one. The metasurface structure's angular stability up to 20^0 oblique incidence angles makes it useful for beam scanning antennas. CST Microwave Studio program is utilized to carry out extensive simulations. This presented study offers a low cost, relatively high-performance, ultrathin polarization converter capable of linear-to-linear and circular polarization conversion in the X-, Ku-, and K-bands.

Keywords:

- Circular Polarization
- Linear Polarization
- Metasurface
- Polarization converter

[1] Seher Şeyma ARSLAN MADAK (**Orcid ID:** 0009-0009-5795-8221), Ramazan TOPKAYA (**Orcid ID:** 0000-0002-5376-0199), Iğdır University, Faculty of Engineering, Department of Electrical and Electronics Engineering, Iğdır, Türkiye
[2] Ahmet TEBER (**Orcid ID:** 0000-0002-7361-2302), Bayburt University, Vocational School of Technical Sciences, Department of Electricity and Energy, Bayburt, Türkiye

***Corresponding Author:** Ahmet TEBER, e-mail: ahmetteber @bayburt.edu.tr

This study was produced from Seher Şeyma ARSLAN MADAK's Master's thesis.

INTRODUCTION

Metamaterials have revealed unique EM properties not found in materials in nature, not naturally available for uses such as invisible cloaking, negative refractive index, holograms, suppression of electromagnetic interference (EMI) from PCB heatsink (Urul et ai., 2022), and advanced lenses (Itoh & Caloz, 2005; Chen et al., 2016; Nama et al., 2021). Recently, the concept of metasurface, which are two-dimensional expressions of metamaterials, has been introduced for a variety of applications, including microwave absorbers (Gosh et al., 2014), filters (Shi et al., 2018), phase shifters (Antoniades et al., 2003), and applications in higher frequency regions.

Metasurface structures have been garnered significant interest from researchers, recently due to their ability to manipulate the polarization of electromagnetic (EM) waves. This wave manipulation is highly sought after for applications in wireless communication, radar detection, stealth, astrogation, and antenna design. Polarization conversion using metasurface designs has been achieved through anisotropy, including the birefringent effect or chirality with optical activity (Mutlu et al., 2011; Zhang et al., 2016; Zheng et al., 2018).

Both transmissive and reflective type polarization conversion techniques are available in the literature. Transmissive type metasurfaces have recently been investigated for LP-to-CP polarization conversion using chirality. On the one hand, it has also been reported that a reflective type double-layer metasurface structure with a lossless dielectric substrate shows LP-to-CP polarization conversion throughout a wide frequency band (Balanis, 2005). Additionally, anisotropy is more effectively used in reflecting type metasurface-polarization converter. The incoming EM wave interacts with the metasurface, which modifies the incoming wave's phase and causes a polarization alteration (Ma et al., 2014). Reflective type metasurfaces for LP-to-LP polarization conversion have been proposed (Bhattacharyya et al., 2017; Guo et al., 2021; Zheng et al., 2018). However, in adverse weather conditions, and to address phasing and polarization mismatch issues, circularly polarized (CP) waves are preferable to linear polarized (LP) ones. (Zhang et al., 2019).

This paper achieves a reflective-type polarization converter capable of LP-to-CP and LP-to-LP polarization conversion, operating in the X-, Ku-, and K-bands. The suggested polarization converter (SPC) has the properties of being facile, easy-to-implement, ultrathin, single-layer, and multi-functional. The performance and operating principle of the suggested polarization converter are thoroughly investigated. We achieved LP-to-LP conversion with an efficiency above 90% in the frequency range of 12.57GHz-19.30GHz, and an efficiency above 97% in frequencies between 12.90GHz and 19.00GHz. Additionally, LP-to-CP conversion is realized as right-handed circular polarization (RHCP) and left-handed circular polarization (LHCP) in frequencies between 11.52-11.84GHz and 19.83-20.01GHz, respectively. Ellipticity, axial ratio (AR), and |Eco|/|Ecross| parameters were examined, which are critical in determining polarization transformation. It was concluded that LP-to-CP was achieved with a significant agreement between these parameters. The high efficiency of the presented polarization converter was tested by observing the efficiency at AR values close to or below 1dB. The bandwidth of the proposed polarization converter under 3dB was observed to be wide, covering 10.29GHz-12.58GHz and 19.32GHz-20.50GHz. Meanwhile, the bandwidth of the proposed polarization converter ranges from 11.52GHz to 11.84GHz under AR=1.12dB, and from 19.83GHz to 20.01GHz at AR=1.46dB. The suggested polarization conversion device can be utilized for military radar applications and other possible uses, such as facilitating the switching between uplink and downlink polarization states for wireless communication in space.

MATERIALS AND METHODS

The materials, designation parameters, and stages of the presented polarization converter are detailed. First, the materials and design procedure are provided, followed by the proposed methodology underlying the polarization conversion.

Materials and Design Procedure

The symmetric unit cell structure of the polarization converter, which consists of four stages, contains a single layer of copper (pure)-FR4 substrate-copper (pure) configuration where FR4 is a composite material consisting of a flame resistant (self-extinguishing) glass-reinforced epoxy resin binder and a woven fiberglass fabric. FR4 thickness is choosen as h=1.6mm (=0.067λ_0 where λ_0 is the wavelength based on the lower frequency of microwave absorption). In the created unit cell, copper is also use on top and bottom layers, with a thickness of 35microns and a conductivity of $\sigma=5.96x10^{-7}$S/m as a metallic layer. The bottom surface is entirely covered by the pure copper.

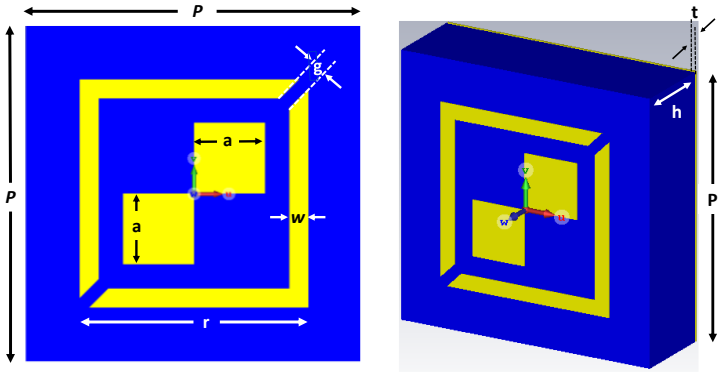

(a) (b)

Figure 1. The SPC with design parameters (a) frontal view and (b) perspective view

As is well knowledge, comprehensive optimization of geometric parameters, such as substrate thickness, size, and shape, is necessary to achieve the optimal configuration with acceptable absorption capabilities. In our design, two identical square shapes were created. In addition, a rectangular block in diagonal position (rotated by degrees) were substracted from the created square ring structure. After these processes, three metallic surfaces were combined. Finally, the PC structure was created (Figure 1). Table 1 contains a list of the design parameters.

Table 1. Best-performing polarization converter design parameters for polarization conversion (in mm)

a	g	h	P	r	W	t
1.05	0.2	1.6	5	2.4	0.6	0.035

Meanwhile, the best results of polarization conversion were obtained by performing simulations at different stages (from Stage 1 to Stage 4) as illustrated in Figure 2. The plotted polarization conversion ratio and reflection coefficients for each stage are going to be discussed in the Results and Discussion section.

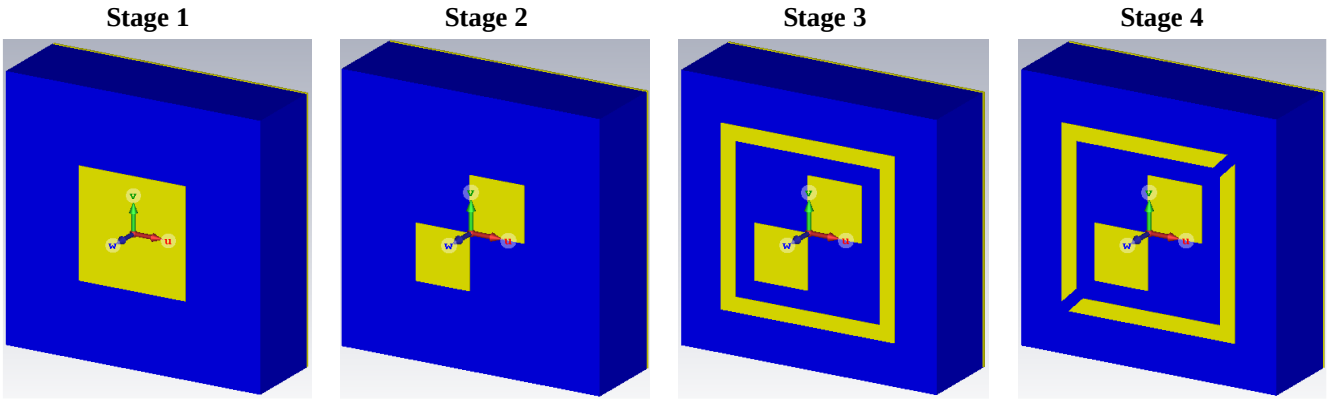

Figure 2. Design stages of the SPC

Mechanism of Polarization Conversion

In order to best (or better) polarization conversion, the optimal design is achieved by optimizing various parameters, as outlined in a parametrical investigation. The effectiveness of polarization conversion is quantified by the parameter of polarization conversion ratio (PCR), defined as follows (Khan et al., 2019; Mao et al., 2017):

$$PCR = \frac{|R_{xy}|^2}{|R_{xy}|^2 + |R_{yy}|^2} \tag{1}$$

where R_{xy} and R_{yy} represent the magnitude of reflection coefficients (RCs) in the *x*- and *y*-directions, indicating S-parameters, simultaneously.

$$R_{xy} = \frac{|E_{rx}|}{|E_{iy}|} \text{ and } R_{yy} = \frac{|E_{ry}|}{|E_{iy}|} \tag{2}$$

These parameters of R_{xy} and R_{yy} are expressed as the cross-polarization RC, and co-polarization RC, respectively whereas E implies electric field, i presents the incident EM wave and r presents the reflected wave. Due to the diagonal symmetry of the proposed design, the magnitude and phase of the cross- and co-polarized reflection waves are similar when the incident wave is along *x*- and *y*-axis. Namely, the reflection coefficients of the reflected wave field, E_r for x-polarized incoming electric field are written for cross- and co-polarized components as given below:

$$r_{yx} = \frac{|E_{ry}|}{|E_{ix}|} \text{ and } r_{xx} = \frac{|E_{rx}|}{|E_{ix}|} \tag{3}$$

From this perspective, the most effective evaluation of a circular polarization converter's ability to maintain circular polarization is through the polarization-maintaining ratio (PMR). When a right-handed circular polarization (RHCP) is present in the reflected wave, the PMR can be explained as following formula (Ahmad et al., 2022):

$$PMR = \frac{|r_{++}|^2}{|r_{++}|^2 + |r_{-+}|^2} \tag{4}$$

where positive notation (+) signifies that the reflected wave is a RHCP, while negative notation (-) denotes a left-handed circular polarization (LHCP). When the PMR is written for LHCP, + and – subscripts are flipped. For the co- and cross-polarized field components of the reflected waves from the metasurface, the co-polarized reflected wave has the same polarization with the incoming wave,

where the cross-polarized reflected wave has polarization as orthogonal component of incoming wave polarization.

The Jones reflection coefficient matrix R (Coskun et al., 2022) in Cartesian coordinates is mathematically employed to analyze co- and cross-polarizations. Here, we refain from providing the details of the analysis of co- and cross-polarizations to avoid repetitition. It is essential to determine the type of circular polarization (RHCP or LHCP) if it is confirmed that circular polarization is occuring. In such cases, ellipticity is derived from the Stokes parameters, which is the crucial parameter in determining the type of polarization converter.

$$e = \frac{2|R_{xy}||R_{yy}|\sin\Delta\varphi}{|R_{xy}|^2+|R_{yy}|^2} \quad (5)$$

where $\Delta\varphi = \varphi_{yy} - \varphi_{xy}$ is the phase difference between co- and cross- reflection polarizations ($\varphi_{yy}\ and\ \varphi_{xy,}\ respectively.$) Based on ellipticity parameter (e), e can be ±1. When e=+1 in the condition of $|R_{xy}| = |R_{yy}|$ and $\Delta\varphi = +90 + 2k\pi$, we make sure that the reflected wave has right-handed circular polarization. When e= -1 in the condition of $|R_{xy}| = |R_{yy}|$ and $\Delta\varphi = -90 + 2k\pi$, it is ensured that the reflected wave has a left-handed circular polarization. Here, k is an integer value for both circumstance.

The $|E_{co}|/|E_{cross}|$ parameter, which is defined as $|R_{yy}|/|R_{xy}|$ determines the circular polarization converter's bandwidth besides the ellipticity parameter. When the unity value is obtained from this ratio, the ellipticity parameter of e becomes ±1, refering to the $\sin\Delta\varphi$ term in Equation 4. The efficiency of a circular polarization converter is predictable when the $|E_{co}|/|E_{cross}|$ parameter are in the range of 0.85-1.15 interval. The phase difference should be in this range from $n90^0 \pm 5^0$, where n is an odd number. Therefore, the bandwidth of polarization converter is obtained by using this interval.

Another crucial parameter to observe the efficiency of the polarization converter is an axial ratio (AR) in dB scale (Xu et al., 2018). It measures a converter ability for circular polarization for the *y*- and *x*-polarized wave. The AR reaches 0dB in the condition of $\Delta\varphi = \pm 90 + 2k\pi$ and $|R_{xy}| = |R_{yy}|$. Then, it can be said that the reflected wave has circular polarization. In the literature, 3dB is taken as a reference point to observe the efficiency of the polarization converter. However, a polarization converter can be high performance features when the AR reaches 1dB and/or under 1dB.

$$AR = \sqrt{\frac{|R_{xy}|^2+|R_{yy}|^2+\sqrt{\tau}}{|R_{xy}|^2+|R_{yy}|^2-\sqrt{\tau}}} \quad (6)$$

$$\tau = |R_{xy}|^4 + |R_{yy}|^4 + 2|R_{xy}|^2|R_{yy}|^2\cos(2\Delta\varphi) \quad (7)$$

RESULTS AND DISCUSSION

The parameters and analysis results obtained from simulation are examined in categories within this section.

Reflection Coefficients and Polarization Conversion Ratio Based on Design Stages

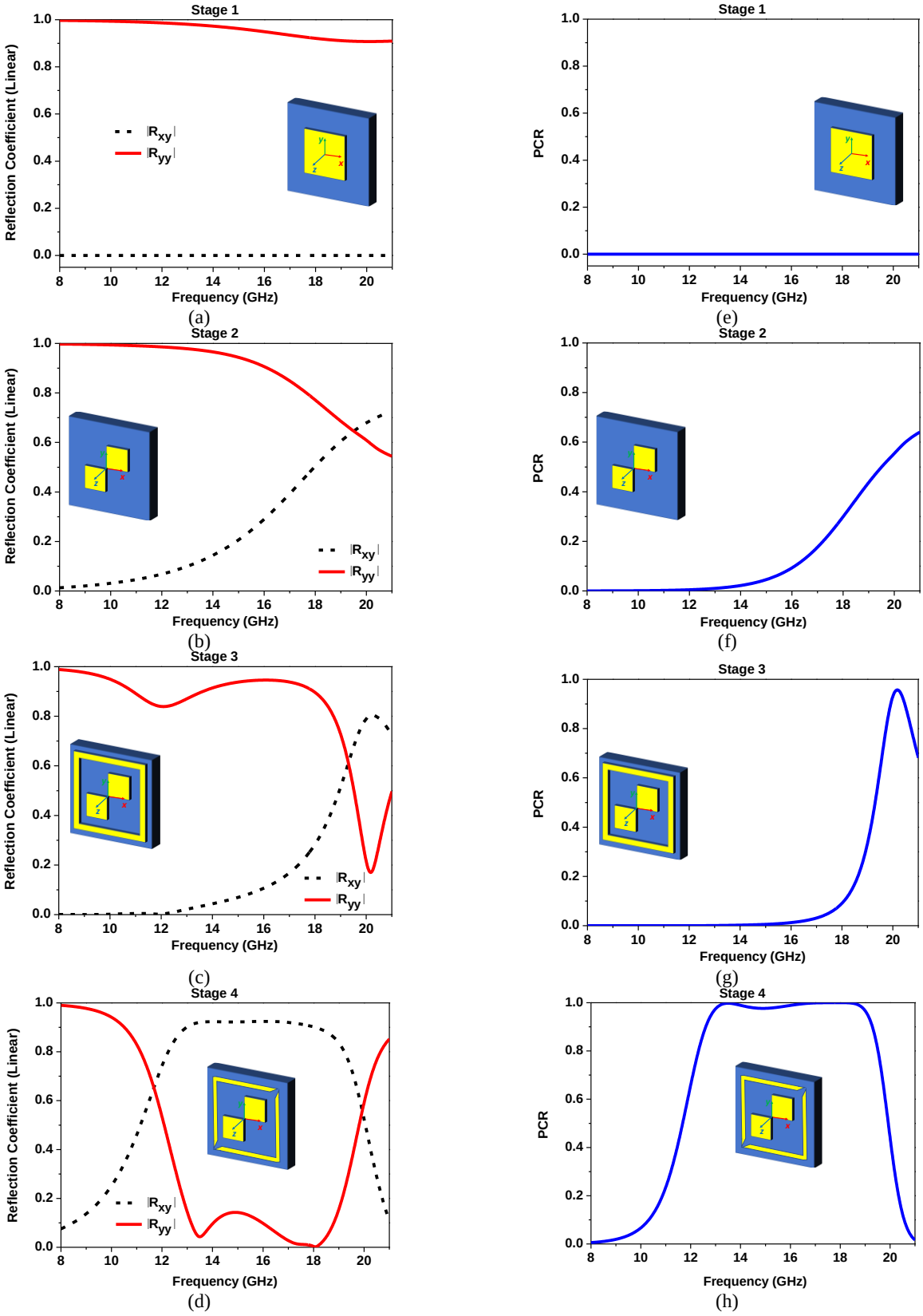

Figure 3. According to the design stages (a-d) Magnitudes of reflection coefficients (e-h) PCR curves

According to the design stages, the impact of architectural changes on the magnitude of the RCs and PCR is examined in Figure 3. The proposed design as shown in Figure 1, is briefly created by following the necessary steps outlined in the geometry given in Figure 3d. Figure 3a-d represent the

magnitude of the reflection coefficients for each stage in detail, while Figure 3e-h exhibit the PCR curves for comparison.

Stage 1 consists of a square layout with a dimension of 2.4 mm centered at the origin. As depicted in Figure 3a, no polarization conversion was observed within the focused frequency region. The structure in the second stage was obtained with creating identical square plates with a length of 1.05mm. Although a single point where the amplitudes of the reflection coefficients were equal occurred above 18GHz, the PCR value was found to be below 0.65. Consequently, no acceptable polarization transformation was achieved at this design stage either (Figure 3b). A square ring of 2.4mm was formed around the structure in the second stage. Thus, the third stage was created to analyze PCR (Figure 3c). Although polarization transformation was achieved in the narrow band in the third stage according to the analysis results, this result is not sufficient for the purpose of this study. A rectangular block in a diagonal position (rotation angle 45^0) was removed from the square ring structure formed, and the last stage structure (Stage 4) was formed in Figure 3d. Based on PCR curve, the reasonable polarization conversion is achieved in the frequency range investigated.

Magnitude and Phase Analysis of Co-and Cross-Polarized Reflection Coefficients

During the simulations using CST Microwave Studio program, the reflection coefficients and phase data are obtained when utilizing the tetrahedral meshing. This type of meshing is carried out in the specified frequency range by automatically choosing the number of meshing cells per unit wavelength.

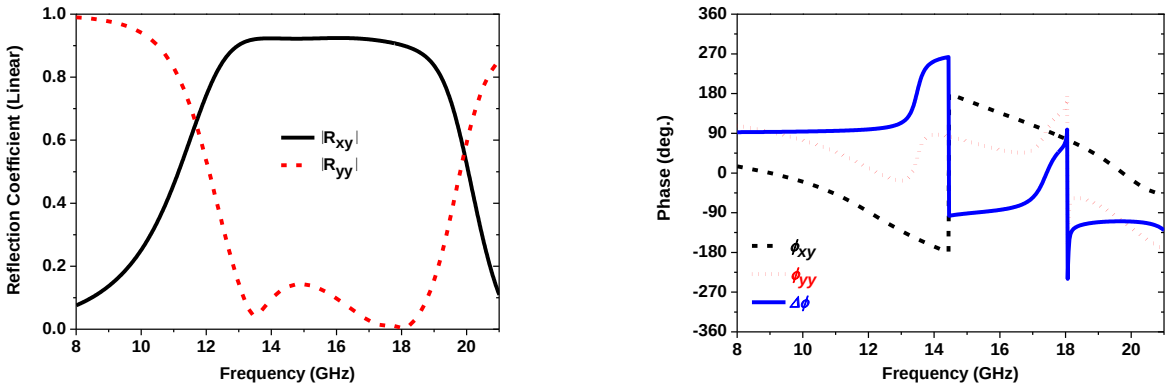

(a) (b)

Figure 4. (a) The magnitude ($|R_{xy}|$ and $|R_{yy}|$) and (b) Phases and phase difference of co- and cross-polarized RCs of the SPC

The magnitude of RCs for y-polarized wave and their phases, including phase difference are plotted as shown in Figure 4. The magnitude of co-polarization coefficient $|R_{yy}|$ is below 0.14, while cross-polarized RC $|R_{xy}|$ is above 0.85 between 12.57GHz and 19.30GHz (Figure 4a). It is also observed that the condition of $|R_{xy}| = |R_{yy}|$ occurs at 11.65 GHz with the magnitude of 0.65, while the condition of $|R_{xy}| = |R_{yy}|$ occurs again at 19.91GHz with the magnitude of 0.55. The phase differences above are approximately $+90^0$ and -90^0 corresponding to the frequency values (Figure 4b). The fact that the phase differences are collapsed at +/-90 degrees indicates that the linear polarized wave turns into circular polarized when reflected.

Polarization Conversion Analysis with Crucial Parameters

The background on polarization conversion was provided in Materials and Method Section. As well known, polarization conversion can be obtained at different combinations such as LP-to-LP, LP-to-CP, CP-to-CP. From Figure 5a, the PCR is obtained above 90% in the frequency range of

12.57GHz-19.30GHz, while it is determined to be above 97% in the specified frequency range of 12.9GHz-19.0GHz. The results indicate that LP-to-LP conversion is achieved in this frequency range.

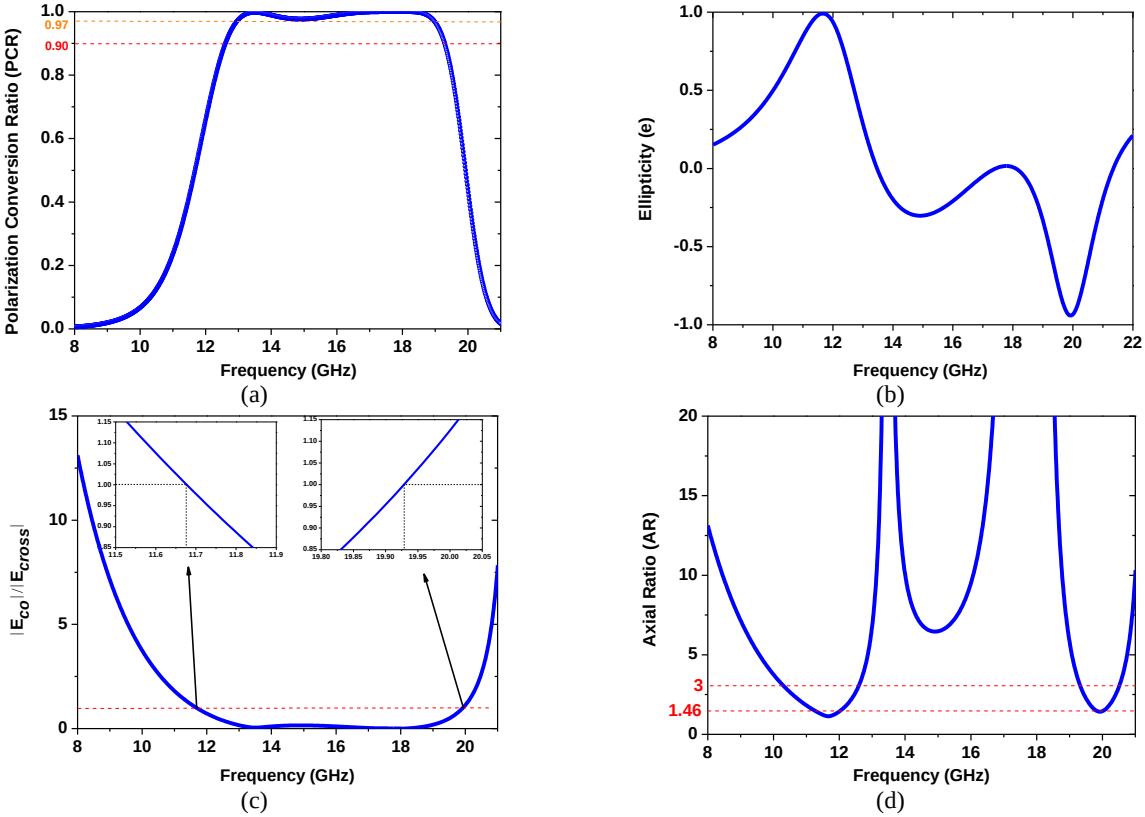

Figure 5. The suggested polarization converter crucial parameters: (a) PCR, (b) ellipticity, e, (c) $|E_{co}|/|E_{cross}|$, and (d) axial ratio, AR in dB

Based on the background, the ellipticity (e) in Figure 5b is calculated using reflection coefficients to understand the type of circular polarization, whether RHCP and/or LHCP. Additionally, $|E_{co}|/|E_{cross}|$is calculated and plotted to confirm the points of RHCP and/or LHCP in Figure 5c. According to the Figure 5b, the ellipticity, e=+1 at 11.68GHz and e=-1 at 19.92GHz when $|R_{xy}| = |R_{yy}|$. These results indicate that the suggested polarization converter performed as an RHCP at 11.67GHz and an LHCP at 19.92GHz. To ensure the ellipticity index results, $|E_{co}|/|E_{cross}|$is plotted. When the ratio of the magnitude of the co-and cross-polarized reflected fields equals the unity value, it becomes an evidence of RHCP and/or LHCP as mentioned in the Materials and Method Section. In the range of 0.85-1.15 of $|E_{co}|/|E_{cross}|$, the bandwidth (BW) of the SPC can be determined for LP-to-CP conversion. As a result, LP-to-CP conversion as an RHCP occurs between 11.52GHz and 11.84GHz, while LP-to-CP conversion as an LHCP is determined between 19.83GHz-20.01GHZ. It should be noted that the frequency points obtained from ellipticity values are the central points of the frequency interval obtained from $|E_{co}|/|E_{cross}|$.

In addition, the axial ratio in dB (AR) is examined to observe the efficiency of the SPC in Figure 5d. It is typically considered below 3dB to determine the operating BW of the circular polarization in the literature. However, it is preferable to observe the efficiency of the polarization converter at AR values close to or below 1dB. This is crucial for determining whether the polarization converter is highly efficient. Under 3dB, the bandwidth of the suggested polarization converter is between 10.29GHz-12.58GHz and between 19.32GHz-20.50GHz. Meanwhile, the bandwidth of the suggested polarization converter changes between 11.52GHz-11.84GHz under an AR of 1.12dB, while it changes

between 19.83GHz-20.01GHz under an AR of 1.46dB. These results correspond with $|E_{co}|/|E_{cross}|$ as predicted.

The operation principle of suggested polarization converter is examined with the illustration in Figure 6.

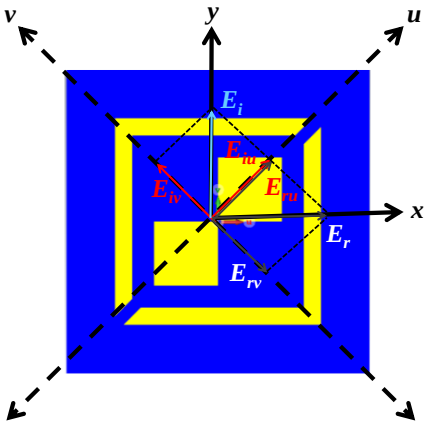

Figure 6. The operation principle of suggested polarization converter, including orthogonal components

The following expressions can use to specify the incoming and reflected waves. Assuming that incoming EM wave (E_i) is directed along *y*-direction, the orthogonal components of (*u*- and *v*-) are inclined to *y*-axis with the rotation angle 45^0 and -45^0, respectively. Thus, the incoming (E_i) and the reflected (E_r) EM waves can be written (Khan et al., 2019) as follows:

$$E_i = \hat{y}E_i = \hat{u}E_{iu} + \hat{v}E_{iv} \tag{8}$$

$$E_r = \hat{u}E_{ru} + \hat{v}E_{rv} = \hat{u}r_uE_{iu} + \hat{v}r_vE_{iv} \tag{9}$$

where $\hat{u}$- and $\hat{v}$- components are the unit vectors, while r_u and r_v are the complex reflection coefficients in the *u*- and *v*-directions, respectively. When E_r is rewritten as an extended form as follows (Khan et al., 2019):

$$E_r = \hat{u}(r_{uu}E_{iu}e^{i\varphi_{uu}} + r_{uv}E_{iv}e^{i\varphi_{uv}}) + \hat{v}(r_{vv}E_{iv}e^{i\varphi_{vv}} + r_{vu}E_{iu}e^{i\varphi_{vu}}) \tag{10}$$

where r_{uu}, r_{uv}, and r_{vv}, r_{vu} are the magnitude of co- and cross-reflection coefficients, while φ_{uu}, φ_{uv} and φ_{vv}, φ_{vu} are the phases of co- and cross-reflection coefficients in the *u*- and *v*-directions, respectively.

When $|r_{uu}| = |r_{vv}| \approx 1$, $|r_{uv}| = |r_{vu}| \approx 0$, and $\Delta\varphi = \varphi_{uu} - \varphi_{vv} = \pm 180^0 + 2k\pi$, (k is an integer) (Nguyen et a., 2021), the synthetic fields of E_{ru} and E_{rv} would become in the x-direction. Thus, the incoming polarized wave rotates 90^0, resulting in CP conversion. LP-to-CP conversion can be attained if $\Delta\varphi = \varphi_{uu} - \varphi_{vv} = \pm 90^0 + 2k\pi$ (k is an integer). It should be noted that the values where the magnitudes of the R_{uu} and R_{vv} are above 0.8 are sufficient to meet the condition. In addition, for the LP-to-LP converter's circumstances, it is stated that $|r_{uu}| = |r_{vv}| \approx 1$ and $\Delta\varphi = \varphi_{uu} - \varphi_{vv} = \pm 180^0$. An LP-to-LP conversion is then verified. From this perspective, the magnitude and the phase of the RCs of the orthogonal components for the normal incidence angle are simulated to assess the property of the suggested converter. Figure 7 is plotted to show the variation of simulated *u*- and *v*- axis reflection coefficients of $|r_{uu}|$ and $|r_{vv}|$, respectively, as a function of frequency.

From Figure 7a, $|r_{uu}|$ and $|r_{vv}|$are at least 0.8 in all frequency bands, except 18.99GHz-21.00 GHz. Figure 7b shows the φ_{uu} , φ_{vv}, and the $\Delta\varphi = \varphi_{uu} - \varphi_{vv}$ along the frequency in the *u*- and *v*- axis. It can be seen from Figure 7b that φ_{uu} has an acute phase change at frequencies of around 14.20GHz. There is no any acute phase change for φ_{vv} at investigated frequency range. Also, the phase difference of ϕ_{uu}-ϕ_{vv} about $\pm180^0$ along 12.57-19.30GHz. It means that the LP-to-LP conversion is verified. For the region where RHCP occurs, LP-to-CP is achieved in the frequency range of 11.52-11.84GHz when the phase difference is about -90^0. The other LP-to-CP conversion where LHCP occurs is obtained in the frequency range of 19.83-20.01GHz when the phase difference is about $+90^0$. All results exhibit that the suggested converter operates as LP and CP converter.

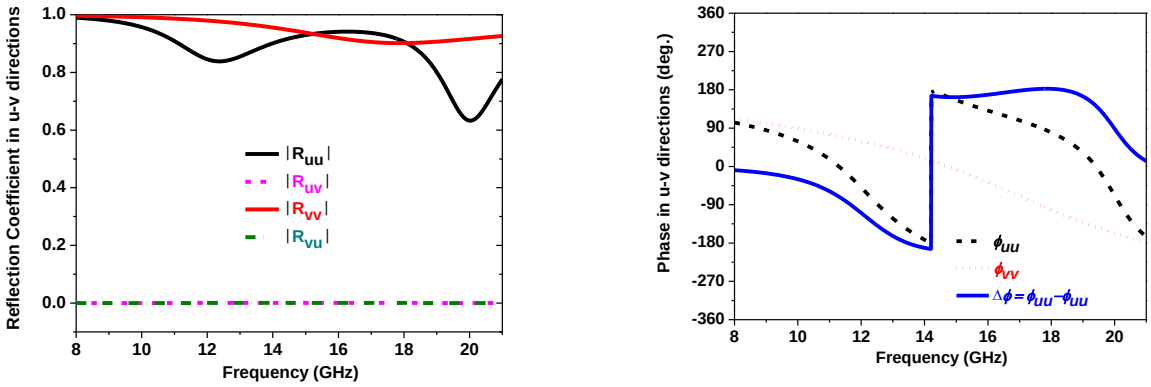

(a) (b)

Figure 7. (a) The magnitude and (b) phase of reflection coefficients on the simulated u- and v-axis under normal incidence

Polarization Conversion Ratio Based on Oblique Incidence Angle

When designing any polarization converter, it is crucial to observe the variation of the PCR based on oblique incidence angle for practical applications. The PCR can be maintanined above 0.84 in the frequency range from 12.38 to 19.44 GHz with the incidence angle up to 20^0 (Figure 8). Above 20^0, the LP-to-LP conversion exhibits a two-band conversion from the broadly elongated distribution.

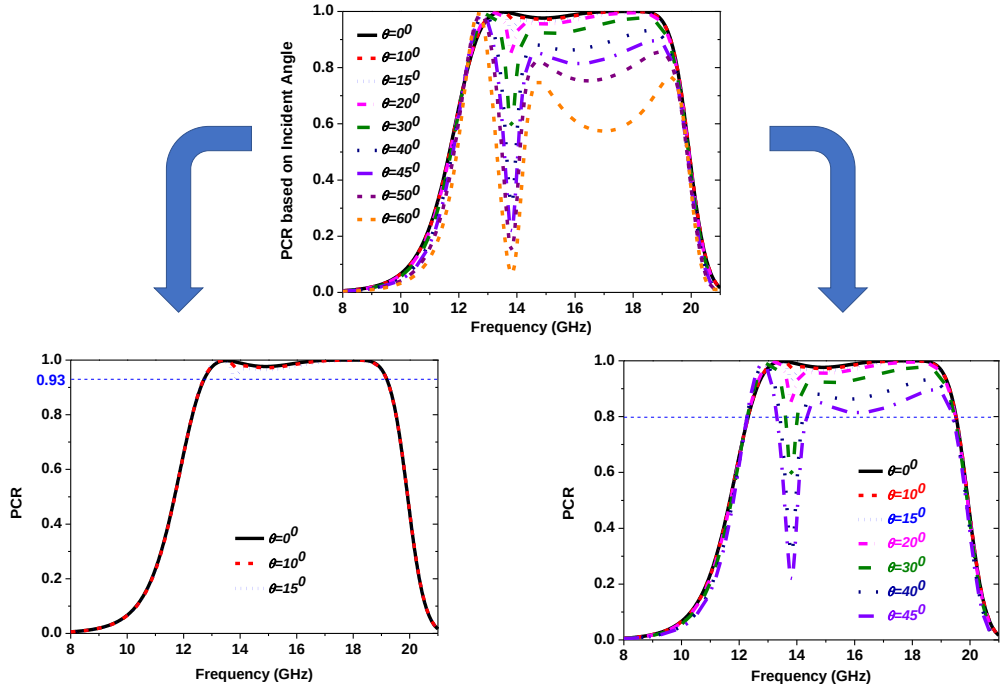

Figure 8. Polarization conversion ratios (PCRs) based on oblique incidence angle, including close view

Based on oblique incidence angle, the PCR observations, with an investigation of the distributions of the bandwidth, are plotted using the magnitude of co- and cross-polarized RCs in

Figure 9 and Figure 10. Specifically, the detailed exhibition of the bandwidth changes is shown in Figure 9, while the distribution of the band widths is shown in Figure 10.

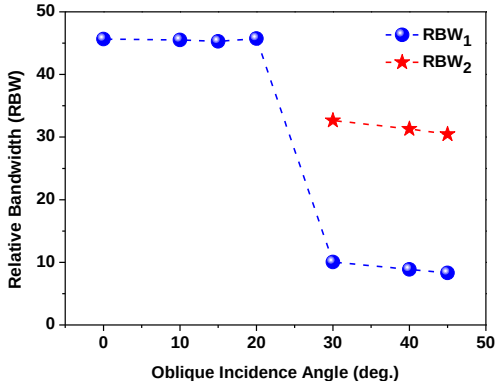

Figure 9. The relative bandwidth (RBW) distribution (uninterrupted RBW is shown in blue color, while devided RBW is shown in red color)

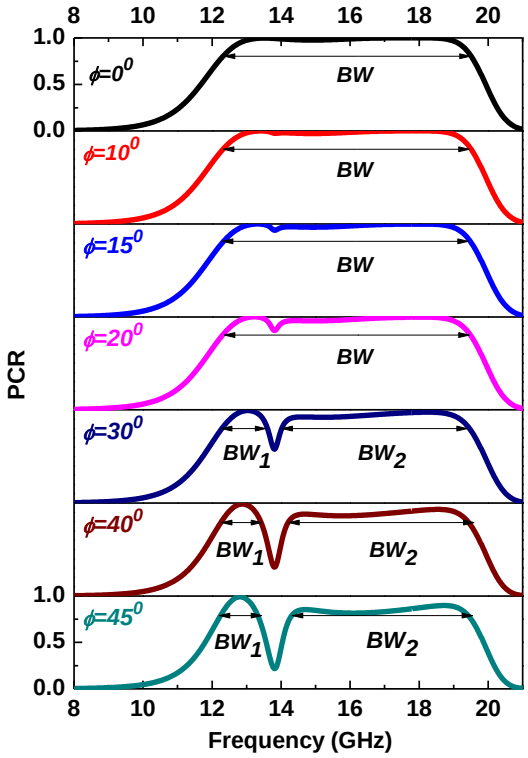

Figure 10. Bandwidths of the suggested polarization converter based on oblique incidence angle

Electric Field and Surface Current Distributions

Understanding the physical mechanism of polarization conversion in the design is important. For this purpose, the surface current distributions on top and bottom surfaces of the suggested PC were examined at the frequencies where resonance occurred. At this point, magnetic resonance is effective in the physical absorption mechanism. The surface current distributions on XoY plane were simulated at the two resonance frequencies of 13.50GHz and 18.19GHz under normal incidence. The surface current distributions of top surface of the suggested polarization converter are presented in Figure 11a and Figure 11b, while Figure 11c and Figure 11d represent the surface current distributions for bottom surface of the suggested polarization converter. The surface current distributions were diagonally analyzed by dividing the unit cell into three regions. Considering that anti-parallel surface currents originate from magnetic resonance (MR) when the purple arrows represent the resultant vector of the black arrows.

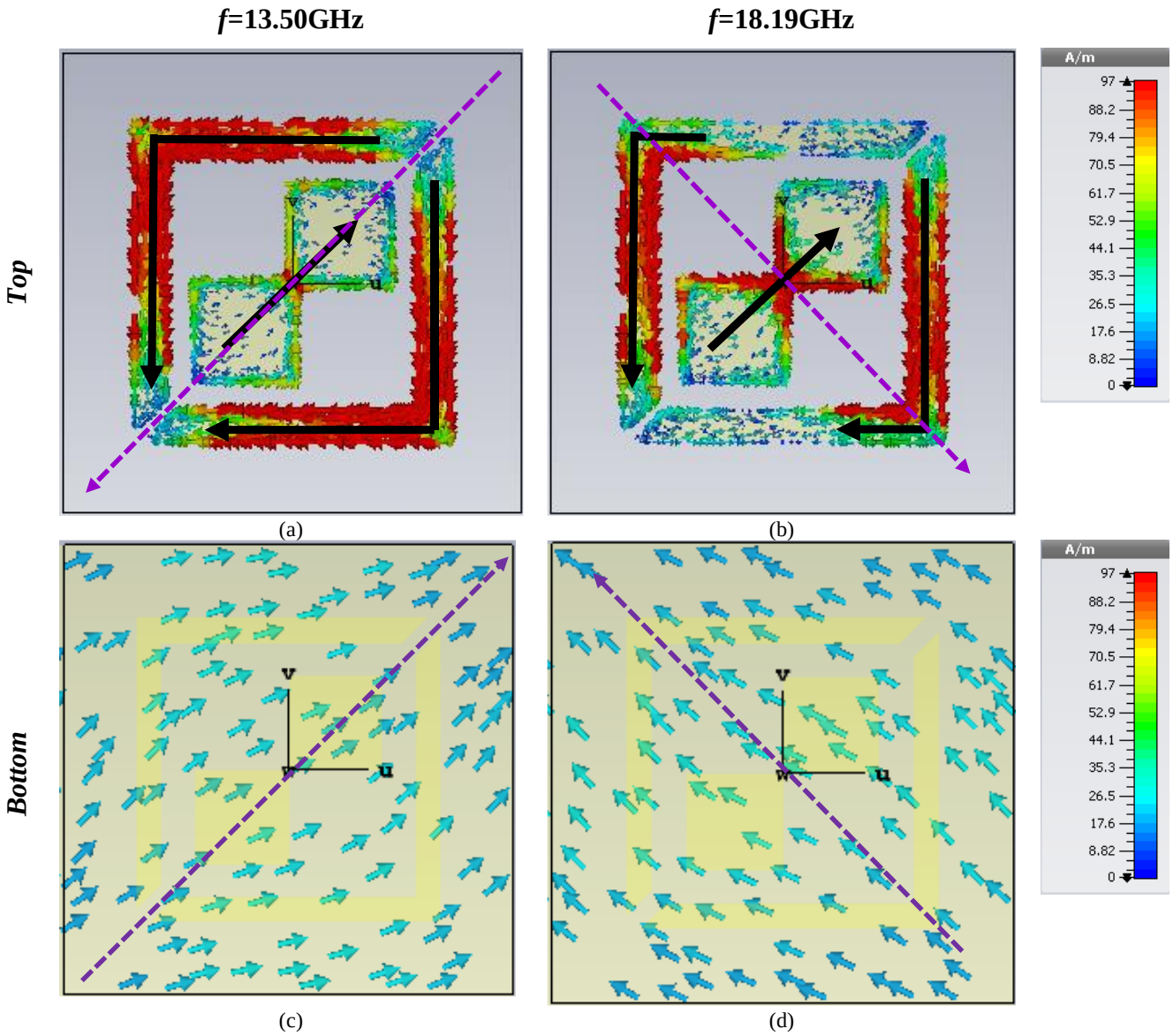

Figure 11. At two peak resonance points of the surface current distributions: (a, b) The top surface of the SPC, (c, d) The bottom surface of the SPC

Parametrical Investigation

As is well-known, both the magnitude and the resonant frequencies can be adjusted by modifying the geometry, dimensions, thickness, and structural parameters. To obtain best results in this study, the optimization parameters for the design, based on a few dimension parameters, are illustrated in Figure 12a through Figure 12d.

The optimization process is carried out obtaining the best polarization conversion ratio (PCR) by modifying the parameters of a, h, P, and r, respectively. For the best conversion and the widest frequency range depending on these parameters, the optimized parameters are choosen as following: P=6.0mm, h=1.6mm, a=1.06mm, and r=2.4mm.

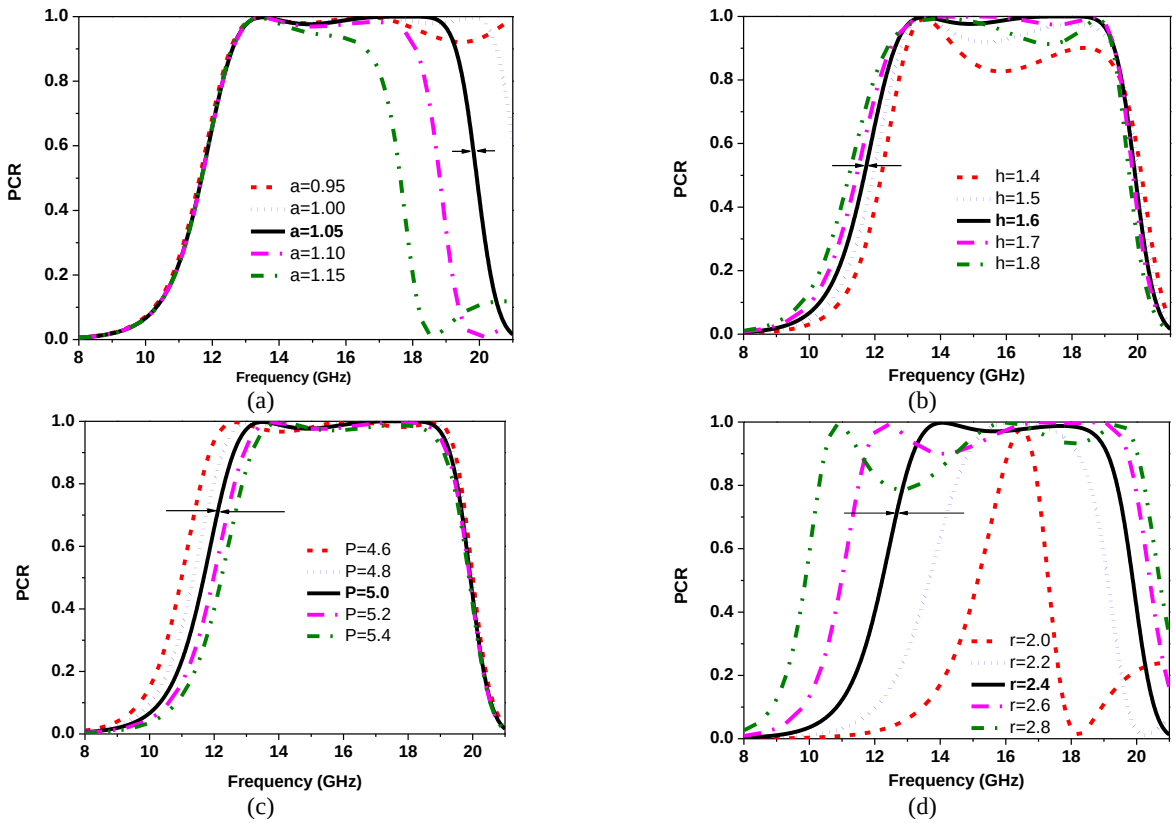

Figure 12. PCR changes of the SPC for various parameters: (a) a=0.95mm-1.15mm, (b) h=1.4mm-1.8mm, and (c) P=4.6mm-5.4mm, and (d) r=2.0mm-2.8mm

Parametric Extraction

The retrieved electromagnetic constitutive parameters, specifically the effective complex permittivity and permeability, are shown in Figure 13a and Figure 13b. Additionally, the effective permittivity (ε_{eff}), effective permeability (μ_{eff}), electric susceptibility (χes), and magnetic susceptibility (χms) can be determined using the following equations (Teber, 2024):

$$\chi_{es} = \frac{2j}{k_0}\frac{1-(S_{21}+S_{11})}{1+(S_{21}+S_{11})} \tag{11}$$

$$\chi_{ms} = \frac{2j}{k_0}\frac{1+(S_{21}+S_{11})}{1-(S_{21}+S_{11})} \tag{12}$$

$$\varepsilon_{eff} = 1 + \frac{\chi_{es}}{d} \tag{13}$$

$$\mu_{eff} = 1 + \frac{\chi_{ms}}{d} \tag{14}$$

where k_0 and d are the wave number and the distance travelled by the incoming wave, respectively. The effective permittivity, permeability, and impedance of the proposed design are extracted using the S-parameter retrieval method, as depicted in Figure 13c. The intrinsic parameters of the metasurface were determined using the following expressions.

$$Z = \pm\sqrt{\frac{(1+S_{11})^2-S_{21}^2}{(1-S_{11})^2-S_{21}^2}} \tag{15}$$

The metamaterial behavior of the proposed structure is also tried to be clarified by giving the PCR and absorption properties of the proposed structure in Figure 13d. The retrieved effective parameters are listed in Table 2.

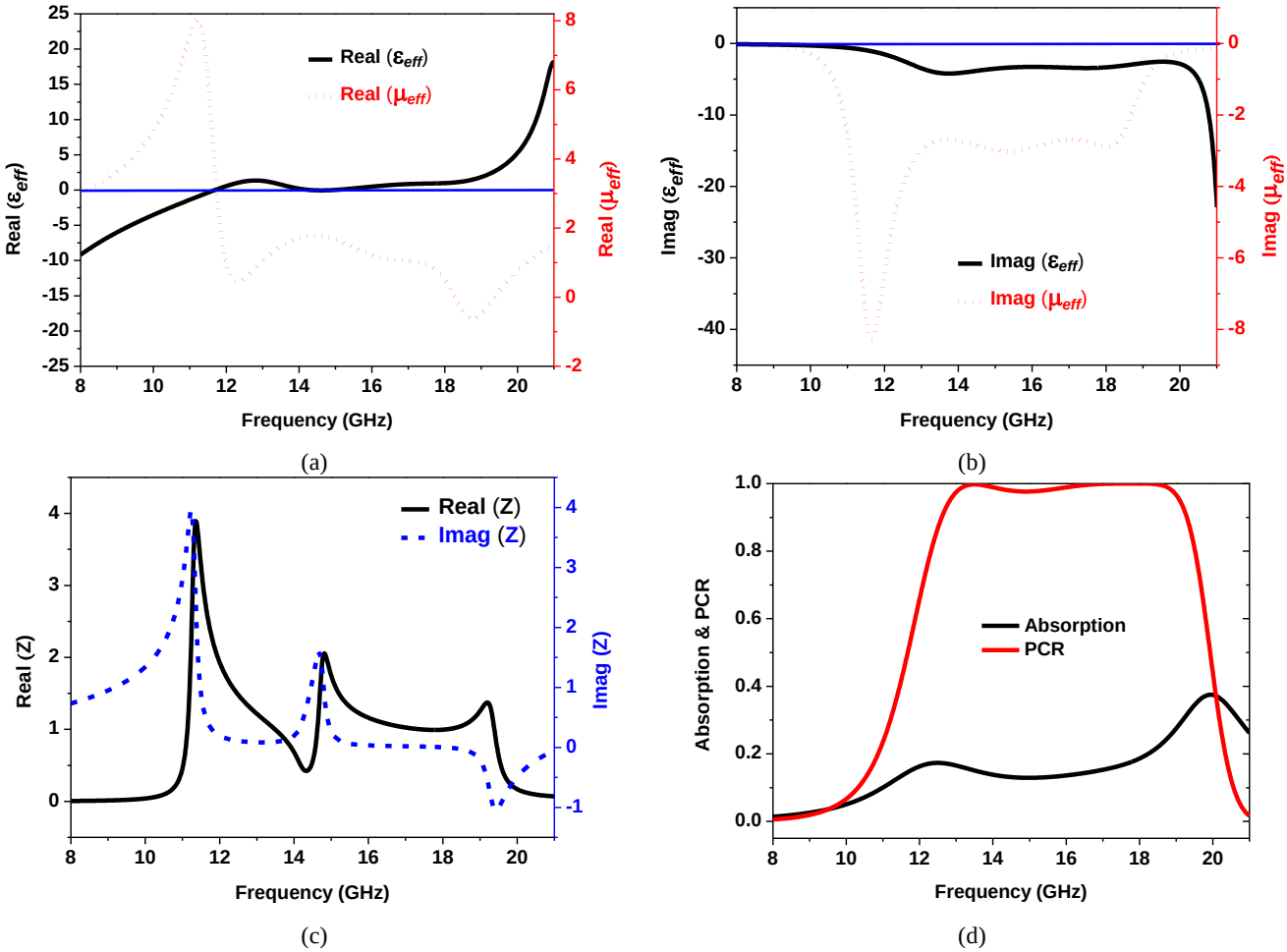

Figure 13. (a) Extracted real parts of effective permittivity and effective permeability, (b) extracted imaginary parts of effective permittivity and effective permeability, (c) the real and imainary parts of impedance of the metasurface, and (d) PCR and absorption characteristics as a functions of frequency of the proposed structure.

The extracted real and imaginary parts of the retrieved permittivity and permeability at 13.32, 17.39, and 18.04 GHz are observed to be nearly equal. This results in impedance matching between the proposed surface and free space, leading to minimal co-polarization reflection and maximum PCR for the proposed surface.

Table 2. Extracted effective parameters of the proposed structure

	Permittivity (ε_{eff})		Permeability (μ_{eff})		Impedance (Z)	
Frequency (GHz)	**Re**	**Im**	**Re**	**Im**	**Re**	**Im**
13.32	1.00	-3.34	1.00	-3.06	0.99	0.090
17.39	0.91	-3.13	1.04	-2.98	0.99	0.010
18.04	1.01	-3.11	1.01	-2.96	1.01	-0.005

Analysis of Performance of the Designed Polarization Converter

The performance analysis of the SPC is presented alongside similar studies regarding focusing on the frequency range. The comparison conditions include the frequency bands investigated, conversion type, the substrate thickness and size, PCR, angular stability, and the name of the operated band name as shown in Table 3.

Table 3. Performance analysis results

References	Thickness (mm and/or λ_0)	Size (mm)	Freq. Band (GHz)	Conversion Type	PCR	Angular Stability	Operated Band Name
(Lin et al.,2019)	$0.087\lambda_0$	9.2x9.2	8.77-24.71	LP-to-CP	Above 0.95	N/A	X, Ku and K
(Couto et al., 2021)	$0.092\lambda_0$	3.64x3.64	13.8-40.70	LP-to-CP	Above 97%	Up to 40^0	Ku, K, and Ka
(Deng et al., 2022)	$0.080\lambda_0$	3.3x3.3	9.34-9.64& 19.14-20.44	LP-to-CP	Above 90%	Up to 30^0	X and K
			10.42-16.72	LP-to-LP	Above 90%	Up to 45^0	Ku
(Nguyen et al., 2021)	$0.060\lambda_0$	6x6	12-18	LP-to-LP	Above 90%	Up to 45^0 Above 80% PCR	Ku
(Faraz et al., 2023)	$0.080\lambda_0$	N/A	10.5-29.5	LP-to-LP	Above 90%	Up to 30^0 Above 88% PCR	X, Ka, and K
(Lu et al., 2021)	2.5mm	10x10	10.63-21.05	LP-to-CP	Above 90%	N/A	X, Ku, and K
(Teber, 2024)	$0.095\lambda_0$	9.8x9.8	9-30	LP-to-CP	Above 90%	Up to 30^0 Above 90% PCR	X, Ku, K, and Ka
(Zhang et al., 2024)	$0.02\lambda_0$	6x6	22-28	LP-to-CP	N/A	Up to 45^0 Above 90% PCR	K and Ka
Proposed Study	**1.6mm ($0.067\lambda_0$)**	**5x5**	**11.52-11.84 & 19.83-20.01**	**LP-to-CP**	**Above 0.9**	**Up to 20^0**	**X and K**
			12.57-19.30	**LP-to-LP**			**Ku**

CONCLUSION

Reflection polarization conversion is achieved using the presented model of the metasurface-based polarization converter. The structure is simple, easy-to-fabricate, ultrathin, and multi-functional, suitable for applications in the X, Ku and K bands. The impact of various structural characteristics is examined to evaluate the mechanism of polarization conversion. In the design, linear-to-linear polarization conversion is obtained with more than 90% efficiency and angular stability of 20^0 between 12.57 and 19.30GHz. Based on oblique incidence, the LP-to-LP conversion is split into two different bands. Additionally, linear-to-circular polarization conversion is generated at 11.52-11.84GHz (as RHCP) and 19.83-20.01GHz (as LHCP). As the subject of further study, the design can be produced with a modular 3D engraving machine, especially the design with a substrate material thickness of $0.067\lambda_0$. The FR4 PCB boards with this thickness are readily available in the market. Eventually, these simulated polarization converter reveals good performance, which is helpful in X, Ku- and K-band applications.

Conflict of Interest

The article authors declare that there is no conflict of interest between them.

Author's Contributions

Seher Seyma Arslan MADAK ve Ahmet TEBER are proposed the idea, performed simulation, analysis/computation related parameters in the topic of the presented study. Seher Seyma Arslan Madak writes the manuscript with the help of Ahmet Teber. In addition, Ahmet Teber and Ramazan Topkaya contributed to this study with fruitful discussions and reviewed the manuscript.

REFERENCES

Ahmad, T., Rahim, A.A., Bilal, R.M.H., Noor, A., Maab, H., Naveed, M.A., Madni, A., Ali, M.M., & Saeed, M.A. (2022). Ultrawideband cross-polarization converter using anisotropic reflective metasurface. *Electronics*, 11(3), 487.

Antoniades, M.A. and Eleftheriades, G.V. (2003). Compact linear lead/lag metamaterial phase shifters for broadband applications. *IEEE Antennas and wireless propagation letters*, 2, 103-106.

Balanis, C.A. (2005). Fundamental Parameters of Antennas, *Antenna Theory: Analysis and Design*. (27-104) John Wiley & Sons.

Bhattacharyya, S., Ghosh, S., & Srivastava, K.V. (2017). A wideband cross polarization conversion using metasurface. *Radio Science*, 52(11), 1395-1404.

Chen, H.T., Taylor, A.J., & Yu, N. (2016). A review of metasurfaces: physics and applications. *Reports on progress in physics*, 79(7), 076401.

Coskun, A., Hasar, U.C., Ozmen, A., & Ertugrul, M. (2022). Easy-to-Implement Ultra-Thin, Wide-Band, and Multi-Functional Polarization Converter for K and Ka Band Applications. *Advanced Theory and Theory Simulations*, 5(4), 2100543.

Couto, M.M., Silva, M.W.B., & Campos, A.L.P.S. (2021). A novel ultra-wideband reflective cross-polarization converter based on anisotropic metasurface. *Journal of Electromagnetic Waves and Applications*, 35(12), 1652-1662.

Deng, G., Yu, Z., Yin, Z., Yang, J., & Li, Y. (2022). A miniaturized and wide-angle 3D metamaterial for reflective polarization conversion. *Optical Materials*, 133, 113017.

Faraz, Z., Kamal, B., Ullah, S., Aziz, A., & Kanwal, H. (2023). High efficient and ultra-wideband polarization converter based on I-shaped metasurface for RCS reduction. *Optics Communications*, 530, 129101.

Ghosh, S., Bhattacharyya, S., Kaiprath, Y., & Vaibhav Srivastava, K. (2014). Bandwidth-enhanced polarization-insensitive microwave metamaterial absorber and its equivalent circuit model. *Journal of Applied Physics*, 115(10), 104503.

Guo, Y., Xu, J., Lan, C., & Bi, K. 2021. Broadband and high-efficiency linear polarization converter based on reflective metasurface. *Engineered Science*, *14*(2), pp.39-45.

Itoh, T. and Caloz, C. (2005). Definition of Metamaterials (MTMs) and Left-Handed (LH) MTMs, *Electromagnetic metamaterials: transmission line theory and microwave applications*. (1-3) John Wiley & Sons.

Khan, M.I., Khalid, Z. and Tahir, F.A. (2019). Linear and circular-polarization conversion in X-band using anisotropic metasurface. *Scientific reports*, 9(1), 4552.

Lin, B., Guo, J., Lv, L., Wu, J., Ma, Y., Liu, B., & Wang, Z. (2019). Ultra-wideband and high-efficiency reflective polarization converter for both linear and circular polarized waves. *Applied Physics A*, 125, 1-8.

Lu, J., Cao, X., Gao, J., Zhiyun, Z., & Li, S. (2021). Low RCS Reflective Polarization Conversion Metasurface. In: 2021 International Conference on Microwave and Millimeter Wave Technology ICMMT (1-3). Nanjing, China. https://ieeexplore.ieee.org/abstract/document/9618050

Ma, H.F., Wang, G.Z., Kong, G.S., & Cui, T.J. (2014). Broadband circular and linear polarization conversions realized by thin birefringent reflective metasurfaces. *Optical Materials Express*, 4(8), 1717-1724.

Mao, C., Yang, Y., He, X., Zheng, J., & Zhou, C. (2017). Broadband reflective multi-polarization converter based on single-layer double-L-shaped metasurface. *Applied Physics A*, 123, 1-6.

Mutlu, M., Akosman, A.E., Serebryannikov, A.E., & Ozbay, E. (2011). Asymmetric chiral metamaterial circular polarizer based on four U-shaped split ring resonators. *Optics letters*, 36(9), 1653-1655.

Nama, L., Bhattacharyya, S., & Jain, P.K. (2021). A metasurface-based, ultrathin, dual-band, linear-to-circular, reflective polarization converter: easing uplinking and downlinking for wireless communication. *IEEE Antennas and Propagation Magazine*, 63(4), 100-110.

Nguyen, T.Q.H., Nguyen, T.K.T., Nguyen, T.Q.M., Cao, T.N., Phan, H.L., Luong, N.M., Le, D.T., Bui, X.K., Truong, C.L., & Vu, D.L. (2021). Simple design of a wideband and wide-angle reflective linear polarization converter based on crescent-shaped metamaterial for Ku-band applications. *Optics Communications*, 486, 126773.

Shi, Z., Khorasaninejad, M., Huang, Y.W., Roques-Carmes, C., Zhu, A.Y., Chen, W.T., Sanjeev, V., Ding, Z.W., Tamagnone, M., Chaudhary, K., & Devlin, R.C. (2018). Single-layer metasurface with controllable multiwavelength functions. *Nano letters*, 18(4), 2420-2427.

Teber, A. (2024). Reflective Polarization Conversion with Multi-Functional, Ultrathin Metasurface for Ku-and K-Band Applications. *Gazi University Journal of Science*, 37(2), 774-791.

Urul, B., Doğan, H., Başyiğit, I. B., & Genç, A. (2022). A novel broadband double-ring holed element metasurface absorber to suppress EMI from PCB heatsinks. *Journal of Electrical Engineering and Computer Sciences*,30(6), 2254-2267.

Xu, J., Li, R., Wang, S., & Han, A.T. (2018). Ultra-broadband linear polarization converter based on anisotropic metasurface. *Optics Express*, 26(20), 26235-26241.

Zhang, B., Yang, X., & Liu, X. (2024). Linear to circular polarization converter using ultrathin and Bi-functional metasurface. *Applied Physics A*, 130(6), 1-11.

Zhang, Z., Cao, X., Gao, J., & Li, S. (2016). Broadband metamaterial reflectors for polarization manipulation based on cross/ring resonators. *Radioengineering*, 25(3), 436-441.

Zhang, H., Zhang, F., Sun, F., Heng, Y., & Su, J. (2019). Wideband Circularly Polarized Applications: Design of a compact, traveling-wave-fed loop antenna. *IEEE Antennas and Propagation Magazine*, 62(1), 34-39.

Zheng, Q., Guo, C., & Ding, J. (2018). Wideband metasurface-based reflective polarization converter for linear-to-linear and linear-to-circular polarization conversion. *IEEE Antennas and Wireless Propagation Letters*, 17(8), 1459-1463.